

# Lawrence Berkeley National Laboratory

## Lawrence Berkeley National Laboratory

### Title

Shaping metal nanocrystals through epitaxial seeded growth

### Permalink

<https://escholarship.org/uc/item/24p1h096>

### Authors

Habas, Susan E.  
Lee, Hyunjoo  
Radmilovic, Velimir  
[et al.](#)

### Publication Date

2008-02-17

## Shaping **binary** metal nanocrystals through epitaxial seeded growth

Susan E. Habas,<sup>1,2</sup> Hyunjoo Lee,<sup>1,2</sup> Velimir Radmilovic,<sup>2</sup> Gabor A. Somorjai,<sup>1,2</sup> and Peidong Yang<sup>1,2</sup>

<sup>1</sup>Department of Chemistry, University of California, Berkeley  
Berkeley, CA 94720

<sup>2</sup>Materials Sciences Division, Lawrence Berkeley National Laboratory  
1 Cyclotron Road, Berkeley, CA 94720

Email: p\_yang@berkeley.edu

**Morphological control of nanocrystals has become increasingly important, as many of their physical and chemical properties are highly shape-dependent. Nanocrystal shape control for both single and multiple material systems, however, remains fairly empirical and challenging. New methods need to be explored for the rational synthetic design of heterostructures with controlled morphology. Overgrowth of a different material on well-faceted seeds, for example, allows for the use of the defined seed morphology to control nucleation and growth of the secondary structure. Here, we have used highly faceted cubic Pt seeds to direct the epitaxial overgrowth of a secondary metal. We demonstrate this concept with lattice matched Pd to produce conformal shape-controlled core-shell particles, and then extend it to lattice mismatched Au to give anisotropic growth. Seeding with faceted nanocrystals may have significant potential towards the development of shape-controlled heterostructures with defined interfaces.**

Heteroepitaxy in gas-phase deposition has been extensively studied for the development of functional heterostructures and devices. The same degree of control is necessary to fully realize the potential of heterostructure formation in solution. The majority of efforts towards solution-phase heterostructure growth have focused on chalcogenide or oxide interfaces,<sup>1-7</sup> or the integration of a metallic component with a chalcogenide or oxide structure.<sup>8-15</sup> Fully metallic heterostructures<sup>12, 16, 17</sup> with controlled shape and interfaces are less well studied.<sup>18-21</sup> Shape control of individual metallic nanoparticles, on the other

hand, has been extensively studied<sup>22-27</sup> and can provide a starting point for the development of shaped heterostructures.

We have focused on the use of faceted metal nanocrystals as nucleation centers for the overgrowth of a secondary metal to obtain shape-controlled metal heterostructures. The effect of seeds on the reduction of metals has been well studied,<sup>28, 29</sup> but little investigation has been done on the effects of seeding with another material.<sup>12, 30, 31</sup> Here, platinum nanocubes (13.4 nm face diagonal with 13% distribution, 9.5 nm edge length, Supplementary Information, Fig. S1)<sup>32</sup> were used as seeds for the reduction of  $K_2PdCl_4$  by ascorbic acid in an aqueous surfactant solution (tetradecyltrimethylammonium bromide, TTAB). The epitaxial overgrowth of Pd on these Pt nanocubes gave Pt/Pd bimetallic core-shell cubes (~75%, 37.2 nm face diagonal with 8% distribution, 26.5 nm edge length). Figure 1a is a scanning electron microscopy (SEM) image showing the overall cubic morphology and monodispersity. The transmission electron microscopy (TEM) image of the array in Figure 1b clearly shows that there is a single Pt nanocube at the center of each core-shell heterostructured nanocube. The X-ray diffraction (XRD) pattern collected on these core-shell nanocubes can be indexed to a face-centered cubic lattice, as Pd and Pt have a small lattice mismatch of only 0.77% that cannot be resolved by our diffractometer. In the absence of seeds, no shape control was observed; instead, a mixture of large particles (>100 nm) including non-polyhedral particles, rods, and various faceted particles, was formed (Fig. S2a). Therefore, the cubic Pt seeds serve two purposes here; they provide a well-defined surface for the overgrowth of the secondary metal, while at the same time dictating the final shapes of the core-shell heterostructures.

Visualizing the orientation of the cubic Pt seed within the cubic Pd shell as well as understanding the nature of the bimetallic interface is difficult for the fully embedded structure in which both components exhibit high-contrast by traditional TEM imaging. We used high angle annular dark field scanning transmission electron microscopy (HAADF-STEM) to analyze the orientation of the two sub-structures. Using this method, the Pt cores stand out sharply in relation to the Pd shells due to the enhanced contrast from the difference in atomic numbers between the two elements (Z-contrast imaging).

Figure 1c shows the intense contrast from the Pt cube centered within the Pd shell which exhibits much lower intensity. Tomographical information, including the mutual orientation of the core and shell, can be extracted from the HAADF-STEM intensity data. Integration of the intensity profile across the face of the Pt/Pd core-shell cubes indicates that the  $\{100\}$  planes of both the Pt core and Pd shell lie at  $\sim 90^\circ$  to one another as expected for the intersection of  $\{100\}$  planes in a cube. We can also see that the Pt cube is oriented with the  $\{100\}$  faces parallel to the  $\{100\}$  faces of the Pd shell as modeled in Figure 1d. The axes extend along the  $\langle 100 \rangle$  directions through the  $\{100\}$  faces of the Pt core. Development of the conformal Pd shell occurs early in the reaction which can be seen by stopping the progress of the reaction before reduction is complete. After five minutes of growth, the cubic Pd shell is fully formed but less than 4 nm thick (Figs. S3a and b). Therefore, we can conclude that epitaxial overgrowth of cubic Pd shells on cubic Pt seeds occurs conformally with balanced growth along the  $\langle 100 \rangle$  and  $\langle 111 \rangle$  directions from the  $\{100\}$  terminated cubic Pt seeds.

To understand the epitaxial nature of the core-shell interfaces within the Pt/Pd nanocubes we have carried out additional high resolution TEM (HRTEM) imaging. The HRTEM image in Figure 2a exhibits negligible contrast between the core and the shell of the Pt/Pd cube because of the high-degree of alignment on the  $\langle 100 \rangle$  zone axis (the expected Pt/Pd interface is shown as a dotted line). However, local distortions of the lattice at the buried interface can be extracted by constructing a phase-image, and then a moiré image that corresponds to the positions of the atomic planes. The moiré images in Figures 2b and c were constructed from the phase images obtained using the (002) and (020) reflections in the Fourier transform of the HRTEM image in Figure 2a. Analysis of the moiré images indicates that the Pt/Pd interface is fully coherent and epitaxial without observable defects. Both the (002) and (020) constructions show parallel phase intensities extending through the expected Pt/Pd boundaries of the core without exhibiting any displacement. Distortions of the patterns occur in the lower left quadrant of Figure 2b and the top of Figure 2c but are not associated with the interfacial region and are probably a result of local surface damage and/or contamination.

Our understanding of the overgrowth process and the epitaxial interface of the Pt/Pd cubes suggests that the defined structure of the Pt seed has a direct influence on the controlled overgrowth of Pd from the epitaxial interface. Extending our control of the directed overgrowth on Pt nanocubes to include shape control chemistry can allow for the utilization of the conformal epitaxial growth to produce core-shell particles with other well-defined shapes. Nitrogen dioxide is known to dissociate on Pd surfaces to give adsorbed NO and adsorbed atomic oxygen. The NO desorbs between 230 and 300K leaving behind adsorbed oxygen,<sup>33</sup> which may interact selectively with the Pd surfaces of the growing particles.<sup>34</sup> By adding NO<sub>2</sub> we were able to vary the growth rates along the <100> and <111> directions to give cuboctahedrally (~90%, 36.4 nm measured body diagonal, with 6% distribution) and octahedrally shaped Pd shells (~90%, 34.6 nm measured 2D projection of body diagonal with 6% distribution, 40.8 nm calculated body diagonal). The cuboctahedral particles imaged by SEM in Figure 1e have a more spherical morphology than that shown by TEM (Fig. 1f). A hexagonal projection for particles oriented on their <111> zone axis can be readily seen in Figure 1f. The SEM image of the octahedra (Fig. 1i) shows particles that are significantly less spherical than the cuboctahedra and have prominent vertices. Analysis by TEM (Fig. 1j) also shows particles that have a hexagonal projection, but unlike the cuboctahedra that pack hexagonally with no overlap, the octahedra overlap at each of their vertices in a manner characteristic of their geometry. Also visible in the TEM images are the presence of the Pt seeds at the core of each structure.

Here we have used the decomposition of concentrated HNO<sub>3</sub> in the presence of concentrated HCl (aqua-regia) as an NO<sub>2</sub> source, although similar results can be obtained by bubbling NO<sub>2</sub> gas through the reaction to give octahedrally shaped Pt/Pd particles (Fig. S4). For all samples, the acid concentration was kept constant at 1 mM by the addition of HNO<sub>3</sub> to avoid any influence of pH on the reactions containing acidic aqua-regia. The addition of aqua-regia or NO<sub>2</sub> slows down the reduction rate considerably. Comparative analysis of the UV-Vis spectra for the [TTA]<sub>2</sub>[PdBr<sub>4</sub>] complex formed prior to reduction,<sup>35</sup> and the complex following exposure to NO<sub>2</sub>(g), shows a shift in the absorption maxima from 341 and 252 nm, to 320 nm with a shoulder at 250 nm after NO<sub>2</sub>

exposure. This process also corresponds to a color change from orange to bright yellow. Excessive  $\text{NO}_2$  exposure renders the complex incapable of reduction under the conditions employed here. As the Pd precursor is reduced, the  $\text{NO}_2$  starts to interact with the surfaces of the growing particle. A preferential interaction of  $\text{NO}_2$  with the  $\{111\}$  surfaces may act to partially passivate the  $\{111\}$  surfaces with adsorbed oxygen, limiting growth along the  $\langle 111 \rangle$  directions possibly by altering the interaction of the TTAB surfactant or bromide counterions with the surfaces.<sup>36</sup> As a result, the nanocrystal sample (Fig. 1g) from reaction containing 0.1 mM aqua-regia exhibits increased growth along the  $\langle 100 \rangle$  directions. The resulting cuboctahedral shells are partially terminated by  $\{111\}$  planes as shown in Figure 1h. Analysis of the HAADF-STEM intensity profile across the body diagonal gives a  $123.1^\circ$  angle between the  $\{111\}$  and  $\{100\}$  planes, which agrees well with the expected  $125.3^\circ$  angle. Increasing the amount of aqua-regia to 1 mM allows growth along the  $\langle 100 \rangle$  directions to dominate, giving Pd octahedral shells composed entirely of  $\{111\}$  faces (Figs. 1k and 1l). The Pt/Pd octahedron in Figure 1k is oriented along the  $\langle 111 \rangle$  zone axis with the Pt seed on a three-fold axis giving a hexagonal projection. Halting the reaction before reduction is complete once again shows that overgrowth is epitaxial and conformal, and that growth along the  $\langle 100 \rangle$  direction to give  $\{111\}$  faces already dominates at an early stage for samples containing  $\text{NO}_2$  (Figs. S3c, d). Overgrowth of Pd on small spherical Pt seeds (3.5 nm) in the presence of  $\text{HNO}_3$  (Fig. S2b) or aqua-regia (Fig. S2c), under otherwise same conditions, does not produce the Pt/Pd cubes or octahedra as described above. Therefore, the uniform  $\{100\}$  surface of the seeds enables precise control of the Pd overgrowth direction to give shells of a defined shape.

It is well known that lattice mismatch has a significant impact on the epitaxial growth of heterostructures for gas-phase deposition. For heterostructures with a high-degree of lattice mismatch, the resulting interface is often non-coherent with a large density of defects. Here we extend the epitaxial overgrowth on cubic Pt seeds to a metal with a larger lattice mismatch. The reduction of Au on cubic Pt seeds (4.08% mismatch versus 0.77% for Pt/Pd) results in the formation of anisotropic rods ( $\sim 185$  nm length and  $\sim 25$  nm diameter) shown by SEM in Figure 3a with the high resolution inset showing the

presence of a Pt seed on each rod. Other products in the sample included faceted particles with a seed partially embedded at the perimeter, and twinned particles that initially formed on a facet of the Pt nanocube and then grew to encompass the Pt seed. It is clear that the high lattice mismatch effectively prevents conformal overgrowth on the Pt nanocube, instead giving a heterostructure in which both the seed and the secondary metal are exposed.

We believe that the lattice mismatch rather than the size of the seed gives rise to the non-conformal growth. For example, studies on the effect of Au seed size on Au rod growth have demonstrated the evolution of rods from seeds as large as 18 nm which are presumably encompassed within the rod.<sup>29</sup> Here, however, we have shown anisotropic growth to form gold rods, each containing a single partially embedded platinum cube at the perimeter of the rod (Figs. 3b and c). Following the nucleation of gold on the platinum cube, growth occurs on the high energy gold nucleate, rather than on the platinum seed, as a result of its smaller size and twinning defects. Further growth occurs bi-directionally, resulting in a Pt/Au structure in which both metals are exposed. Reduction does not occur in the absence of seeds, and Au rods produced from smaller spherical Pt seeds (3.5 nm) most likely have seeds enclosed within the rod structure.<sup>31</sup> The gold rods here are also pentagonally twinned as can be seen from the HRTEM image in Figure 3d showing a gold rod viewed down the  $\langle 112 \rangle / \langle 100 \rangle$  zone with continuous  $\{111\}$  fringes running parallel to the long axis. The corresponding SAED pattern (inset) is indicative of a  $\langle 112 \rangle$  zone overlapped with  $\langle 100 \rangle$  zone. The first order reflections labeled *A*, *B*, and *C* correspond to the (1-11), (131) and (220) planes of the rectangular [-112] reciprocal lattice, and those labeled *a*, *b*, and *C*, to the (-200), (020) and (220) planes of the square [001] lattice.<sup>37</sup> In addition to the associated double diffraction reflections, a second smaller set of diffraction spots slightly offset from the gold [-112] zone (Fig. 3d, *B* expanded below inset) can be indexed to the platinum cube epitaxially oriented with one of the five domains of the gold rod.

Shape control enabled by this epitaxial seeding concept allows us to study surface dependent properties such as catalytic activity. Electrochemical oxidation of formic acid

was used to evaluate the catalytic properties of the Pt/Pd core-shell nanocrystals. The effect of surface structure on electrocatalytic activity and selectivity has been extensively studied.<sup>38, 39</sup> Surface reaction selectivity depends on how the arrangement of the atoms and the corresponding energy of the surface affects adsorption, surface diffusion, intermediate formation, chemical rearrangements, and finally desorption of the products. Structural effects on formic acid oxidation were investigated on single crystalline Pd electrodes including Pd(100) and Pd(111).<sup>40, 41</sup> According to Baldauf and Kolb,<sup>40</sup> the Pd(100) single crystal surface showed an anodic peak current approximately four times higher than that for the Pd(111) surface, which corresponds to an increased oxidation rate of formic acid at the Pd(100) surface. However, the Pd(111) surface gave a lower peak potential (0.07 V vs Ag/AgCl) than the Pd(100) surface (0.42 V) for formic acid oxidation. The Pd(100) single crystalline electrode was also found to be more susceptible to oxidation than the Pd(111) electrode. Figure 4 shows cyclic voltammograms for formic acid oxidation on cubes (Fig. 4a), cuboctahedra (Fig. 4b), and octahedra (Fig. 4c). The Pd cubes show a peak current that is five times higher than that observed for the Pd octahedra, while the Pd octahedra have a lower peak potential (0.15 V) than the Pd cubes (0.36 V). The Pd cubes also have a sharper peak in the negative scan than the octahedra, at 0.47 V, corresponding to the reduction of Pd oxide. The Pd cuboctahedra exhibit properties intermediate between the cubes and octahedra.

In summary, we have demonstrated that by controlling the epitaxial overgrowth of a secondary metal on well-faceted cubic Pt seeds, we can produce both conformal shape-controlled overgrowth as well as anisotropic overgrowth depending on the degree of lattice mismatch. This concept could be applied to other material systems (e.g. Rh, FePt, CoPt), creating novel heterostructures for catalysis, optical, and magnetic applications where shape control plays a crucial role.



## Methods

### Growth of Pt seeds

Cubic Pt seeds (13.4 nm face diagonal with 13% distribution) were synthesized as described elsewhere.<sup>32</sup> Briefly, 100 mM aqueous tetradecyltrimethylammonium bromide (TTAB) and 1 mM  $K_2PtCl_4$  (Aldrich, 99.99%) was reduced by 30 mM  $NaBH_4$  at 50°C. Excess  $H_2$  evolved from the reaction of water with  $NaBH_4$  was released by inserting a needle into the septum capping the reaction vessel. After 6 hours, the reaction was allowed to cool to room temperature and left overnight to promote the decomposition of remaining  $NaBH_4$  in water. Platinum nanoparticles were collected after removing larger precipitates by centrifugation. The pH of the seed solution was lowered from ~9 to ~3 to ensure decomposition of residual  $NaBH_4$  by the addition of HCl, and then neutralized with NaOH.

Small spherical Pt seeds (3.5 nm) were also prepared according to a method described previously.<sup>42</sup> Reduction of  $H_2PtCl_6 \cdot 6H_2O$  (0.6 mM, 99.9%, Alfa Aesar) in an aqueous solution of Pluronic L64 ( $EO_{13}PO_{30}EO_{13}$ , BASF) triblock copolymer (6 mM, 10 mL) was achieved by the addition of  $NaBH_4$  (1 mg) while stirring at room temperature in a closed vial. The reaction was left overnight before use.

### Epitaxial overgrowth and shape-control of Pd shells

Conformal overgrowth of Pd on cubic Pt seeds was achieved by introducing Pt seeds (100  $\mu$ L) and *L*-ascorbic acid (50  $\mu$ L of 100 mM solution) into an aqueous solution (5 mL) containing 100 mM TTAB and 0.5 mM  $K_2PdCl_4$  (Alfa-Aesar, 99.99%) that had been heated at 50°C for 5 min. while stirring in a capped vial. The morphology of the Pd shell was altered by increasing the amount of  $NO_2$  added to the reaction conditions described above. This was done either by addition of gaseous  $NO_2$  or a 1:1 volume ratio of HCl (12.1 M) and  $HNO_3$  (15.7 M) (aqua-regia) that had been allowed to react for 4 hours. The addition of aqua-regia in the following concentrations gave cubes (0 mM), cuboctahedra (0.1 mM), and octahedra (1.0 mM). Alternatively, similar results could be obtained by bubbling  $NO_2$  (0.99% in He, Praxair) through  $H_2O$  for 30 min. and then adding 10  $\mu$ L of this solution to the reaction to give Pt/Pd octahedra. For all reactions the total acid

concentration was held constant at 1 mM with the difference made up by the addition of HNO<sub>3</sub>. All acids and NO<sub>2</sub> were added to the TTAB solution before the Pd salt. Cubic samples were removed from heat after 1 hr, and cuboctahedral and octahedral samples after 2.5 hrs.

### **Growth of anisotropic Au rods**

The Au rods were prepared by adding cubic Pt seeds (25 μL) into a solution (5 mL) containing 100 mM TTAB, 0.25 mM HAuCl<sub>4</sub> (99.9%, Alfa-Aesar) and 0.5 mM L-ascorbic acid. The solution was shaken briefly in a capped vial, and Au reduction was indicated by the development of a pale pink color within 30 sec. Reduction was allowed to proceed for at least five minutes to give a deep purple/pink solution. Reactions were performed at room temperature due to the fast reduction of Au by ascorbic acid.

### **Electrocatalytic formic acid oxidation**

Electrochemical measurements were performed in 0.1 M H<sub>2</sub>SO<sub>4</sub> and 0.2 M formic acid at room temperature. A three-electrode cell was used with an Ag/AgCl reference electrode and a gold wire as the counter electrode. The Pt/Pd core-shell nanoparticles (10 mL) were washed and concentrated to 0.1 ml then deposited on a gold foil working electrode and dried for 2 hrs. Cyclic voltammetry (CV) data were collected at a sweep rate of 50 mV/s after stabilizing the CV curve through repetitive scans which acted to remove surfactant molecules from the Pd surfaces.

### **Sample characterization**

The structure and composition of the samples were investigated by XRD (Co K $\alpha$  radiation, D-8 GADDS general area detector, Bruker), SEM (FEI Strata 235 Dual Beam FIB), TEM (JEOL 200CX and Tecnai G<sup>2</sup> S-Twin), HRTEM (Philips, CM200), and HAADF-STEM (FEI monochromated F20 UT Tecnai). Samples were centrifuged and washed with fresh TTAB solution and then water before resuspending in water and drying on a silicon substrate for XRD and SEM, or a carbon coated copper grid for TEM.

## Figure captions

**Figure 1: Electron microscopy characterization of the shaped binary metal nanocrystal.** Well-defined cubic Pt seeds were used to direct the epitaxial overgrowth of Pd to form Pt/Pd core-shell nanocubes. The overall morphology is shown by SEM (a), and TEM (b) indicates the presence of a cubic Pt seed at the core of each particle. Analysis by HAADF-STEM (c) gives the orientation of the cubic Pt seed within the Pd shell. The Pt core stands out sharply in relation to the Pd shell due to the enhanced contrast from the difference in atomic numbers between the two elements. The orientation of the core and shell are modeled (d) with the axes projecting along the  $\langle 100 \rangle$  directions through the  $\{100\}$  faces of the central Pt cube. Control over the directed growth of Pd on Pt nanocubes was achieved by the addition of increasing amounts of  $\text{NO}_2$  which altered the growth rates along the  $\langle 100 \rangle$  and  $\langle 111 \rangle$  directions to give Pt/Pd core-shell cuboctahedra (e-h) and octahedra (i-l). The SEM images (e and i) are provided for clarification of the 3D morphology, and TEM images (f and j) to show the presence of a Pt seed at the core of each particle. HAADF-STEM images give the orientation of the cubic Pt seed within a Pd cuboctahedron (g) and octahedron (k). The Pt/Pd octahedron (k) is oriented along the  $\langle 111 \rangle$  zone axis with the Pt seed on a three-fold axis giving a hexagonal projection. The corresponding models are provided (h and l).

**Figure 2: Phase constructions of a Pt/Pd cube showing a coherent and epitaxial interface between the cubic Pt core and Pd shell.** The (002) and (020) reflections from the Fourier transform of the HRTEM image (a) were used to construct the corresponding moiré images (b) and (c) which indicate that there are no visible distortions through the expected Pt/Pd boundaries, shown by a dotted line in (a).

**Figure 3: Epitaxial overgrowth of lattice mismatched Au on cubic Pt seeds to give anisotropic growth of Au rods.** The SEM image (a) shows an overview of Au rods nucleated from cubic Pt seeds, magnified at inset (scale bar is 100 nm), with TEM image (b) of multiple rods indicating that a single Pt cube is associated with each Au rod. The HRTEM image (c) shows a single Pt cube partially embedded in the side of an Au rod. The length of the rod is shown in (d), viewed down the  $\langle 112 \rangle / \langle 100 \rangle$  zone with

continuous  $\{111\}$  fringes running parallel to the long axis, and the corresponding SAED electron diffraction pattern (inset, discussed in text) with double-diffraction is indicative of a pentagonally twinned particle. The magnified view of the (1-31) reflection (*B*) shows an additional reflection arising from the Pt cube epitaxially oriented one of the five  $[112]$  zones of the Au rod.

**Figure 4: Catalytic activity of the Pt/Pd binary metal nanocrystals.** The effect of surface structure on the catalytic activity of the Pt/Pd core-shell nanoparticles was investigated by electrochemical formic acid oxidation. Cyclic voltammograms for cubes (a), cuboctahedra (b), and octahedra (c) were obtained at a sweep rate of 50 mV/s in 0.1 M H<sub>2</sub>SO<sub>4</sub> and 0.2 M formic acid.

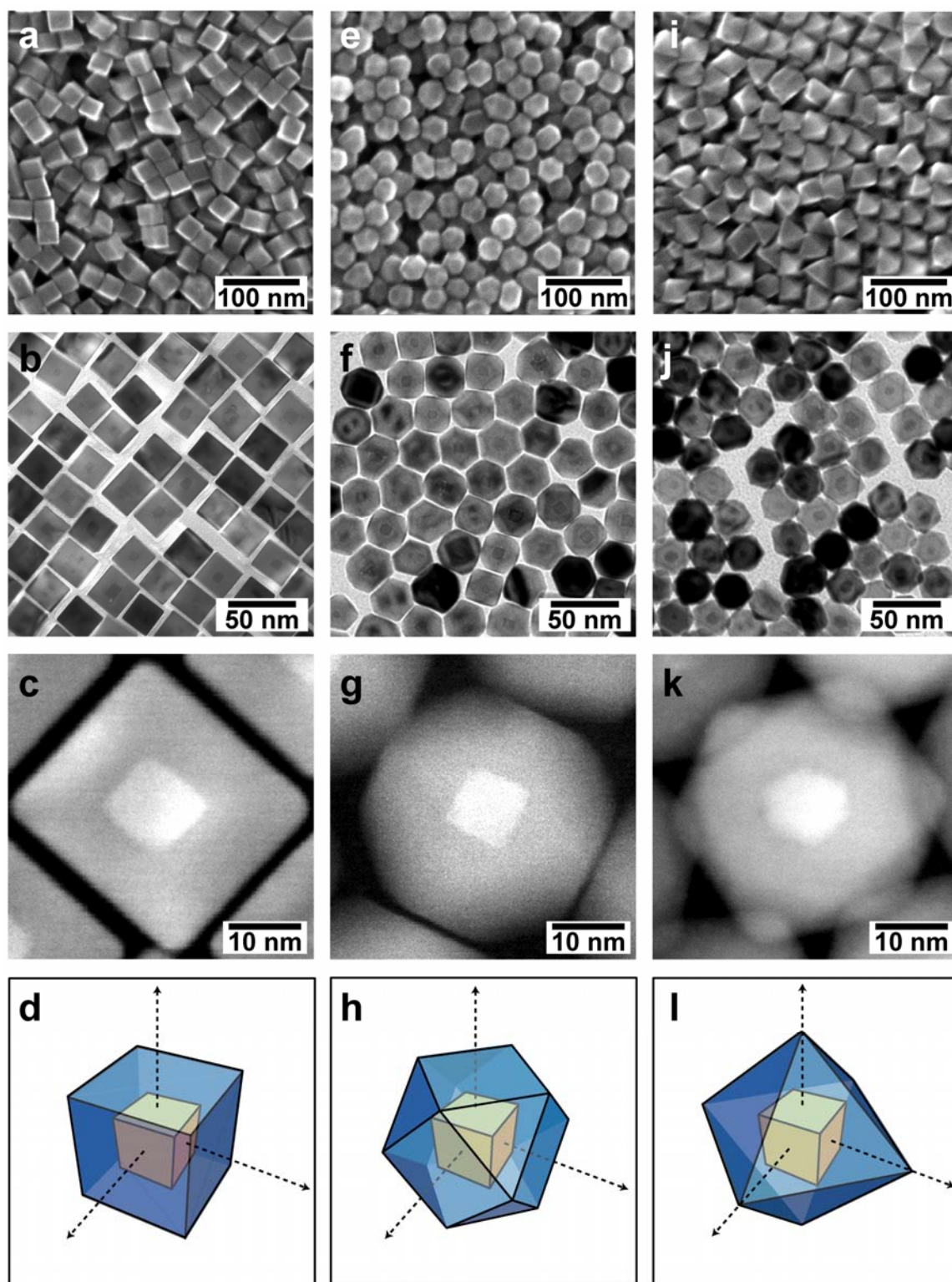


Figure 1

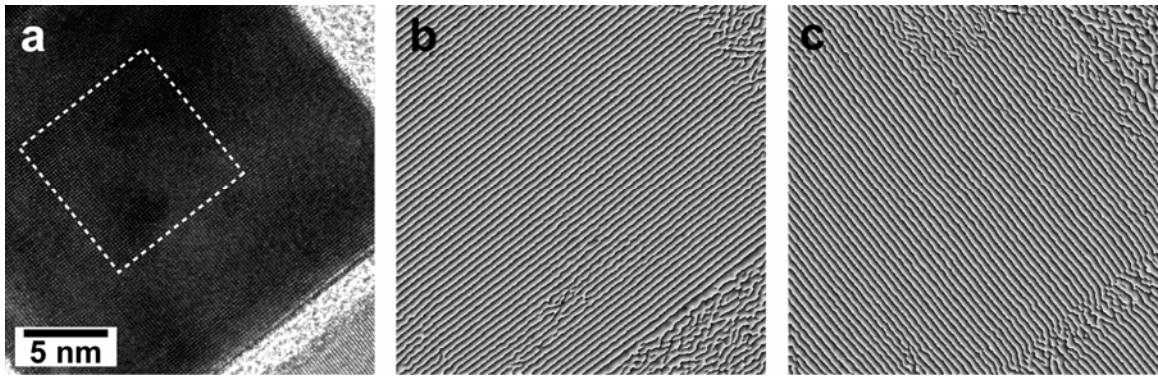


Figure 2

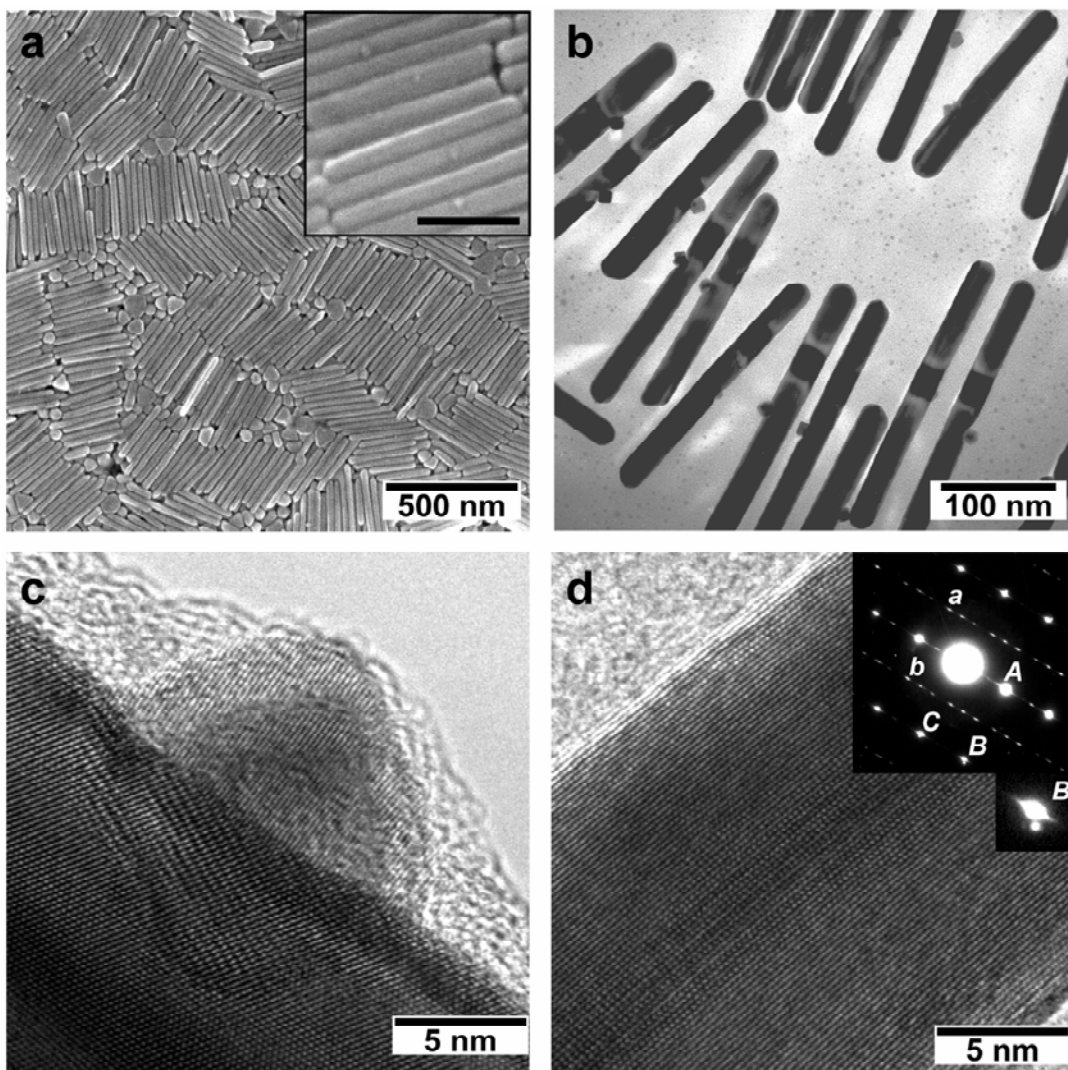


Figure 3

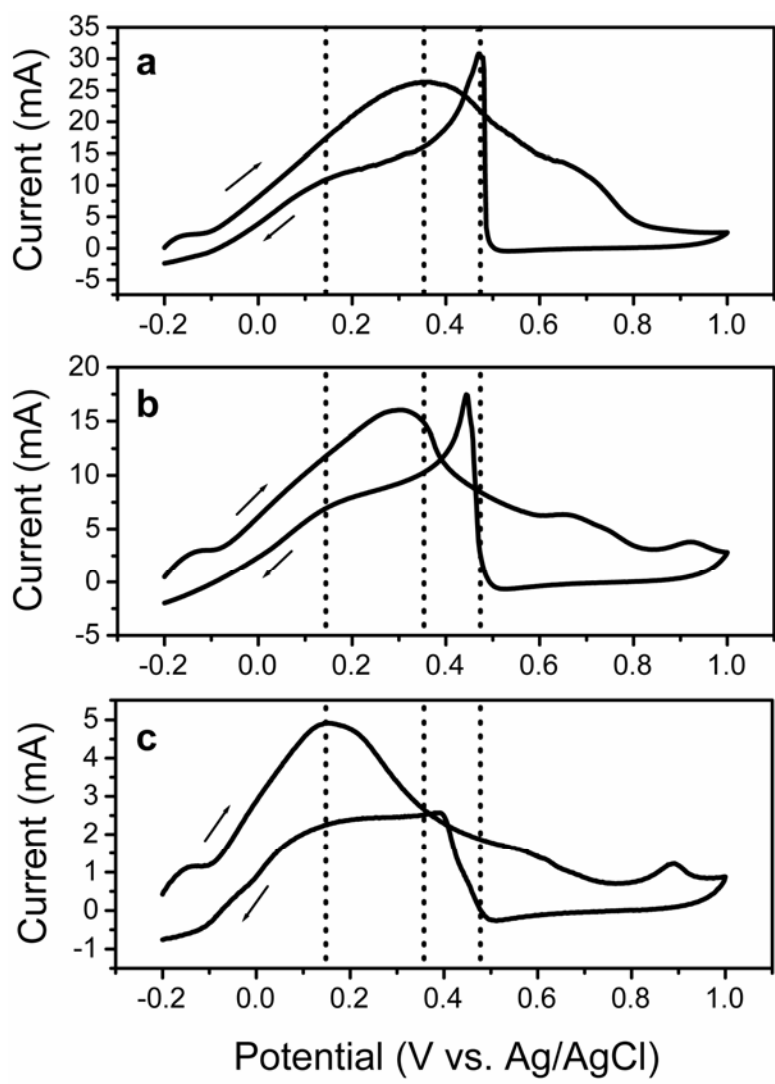


Figure 4



## References

1. Milliron, D. J. et al. Colloidal nanocrystal heterostructures with linear and branched topology. *Nature (London)* 430, 190-195 (2004).
2. Kudera, S. et al. Selective Growth of PbSe on One or Both Tips of Colloidal Semiconductor Nanorods. *Nano Lett.* 5, 445-449 (2005).
3. Buonsanti, R. et al. Seeded Growth of Asymmetric Binary Nanocrystals Made of a Semiconductor TiO<sub>2</sub> Rodlike Section and a Magnetic  $\gamma$ -Fe<sub>2</sub>O<sub>3</sub> Spherical Domain. *J. Am. Chem. Soc.* 128, 16953-16970 (2006).
4. Talapin, D. V. et al. Highly emissive colloidal CdSe/CdS heterostructures of mixed dimensionality. *Nano Lett.* 3, 1677-1681 (2003).
5. Kwon, K.-W. & Shim, M.  $\gamma$ -Fe<sub>2</sub>O<sub>3</sub>/II-VI Sulfide Nanocrystal Heterojunctions. *J. Am. Chem. Soc.* 127, 10269-10275 (2005).
6. Kwon, K.-W., Lee, B. H. & Shim, M. Structural Evolution in Metal Oxide/Semiconductor Colloidal Nanocrystal Heterostructures. *Chem. Mater.* 18, 6357-6363 (2006).
7. Teranishi, T., Inoue, Y., Nakaya, M., Oumi, Y. & Sano, T. Nanoacorns: Anisotropically Phase-Segregated CoPd Sulfide Nanoparticles. *J. Am. Chem. Soc.* 126, 9914-9915 (2004).
8. Mokari, T., Sztrum, C. G., Salant, A., Rabani, E. & Banin, U. Formation of asymmetric one-sided metal-tipped semiconductor nanocrystal dots and rods. *Nat. Mater.* 4, 855-863 (2005).
9. Shi, W. et al. A General Approach to Binary and Ternary Hybrid Nanocrystals. *Nano Lett.* 6, 875-881 (2006).
10. Yu, H. et al. Dumbbell-like Bifunctional Au-Fe<sub>3</sub>O<sub>4</sub> Nanoparticles. *Nano Lett.* 5, 379-382 (2005).
11. Gu, H., Zheng, R., Zhang, X. & Xu, B. Facile One-Pot Synthesis of Bifunctional Heterodimers of Nanoparticles: A Conjugate of Quantum Dot and Magnetic Nanoparticles. *J. Am. Chem. Soc.* 126, 5664-5665 (2004).
12. Gu, H., Yang, Z., Gao, J., Chang, C. K. & Xu, B. Heterodimers of Nanoparticles: Formation at a Liquid-Liquid Interface and Particle-Specific Surface Modification by Functional Molecules. *J. Am. Chem. Soc.* 127, 34-35 (2005).
13. Yang, J., Elim, H. I., Zhang, Q., Lee, J. Y. & Ji, W. Rational Synthesis, Self-Assembly, and Optical Properties of PbS-Au Heterogeneous Nanostructures via Preferential Deposition. *J. Am. Chem. Soc.* 128, 11921-11926 (2006).
14. Casavola, M. et al. Topologically Controlled Growth of Magnetic-Metal-Functionalized Semiconductor Oxide Nanorods. *Nano Lett.* 7, 1386-1395 (2007).
15. Pacholski, C., Kornowski, A. & Weller, H. Nanomaterials: Site-specific photodeposition of silver on ZnO nanorods. *Angew. Chem., Int. Ed.* 43, 4774-4777 (2004).
16. Pellegrino, T. et al. Heterodimers Based on CoPt<sub>3</sub>-Au Nanocrystals with Tunable Domain Size. *J. Am. Chem. Soc.* 128, 6690-6698 (2006).
17. Gao, X., Yu, L., MacCuspie, R. I. & Matsui, H. Controlled growth of Se nanoparticles on Ag nanoparticles in different ratios. *Adv. Mater.* 17, 426-429 (2005).

18. Xiang, Y. et al. Formation of Rectangularly Shaped Pd/Au Bimetallic Nanorods: Evidence for Competing Growth of the Pd Shell between the {110} and {100} Side Facets of Au Nanorods. *Nano Lett.* 6, 2290-2294 (2006).
19. Krichevski, O., Tirosh, E. & Markovich, G. Formation of gold-silver nanowires in thin surfactant solution films. *Langmuir* 22, 867-870 (2006).
20. Tsuji, M. et al. Crystal Structures and Growth Mechanisms of Au@Ag Core-Shell Nanoparticles Prepared by the Microwave-Polyol Method. *Cryst. Growth Des.* 6, 1801-1807 (2006).
21. Sanedrin, R. G., Georganopoulou, D. G., Park, S. & Mirkin, C. A. Seed-mediated growth of bimetallic prisms. *Adv. Mater.* 17, 1027-1031 (2005).
22. Kim, F., Connor, S., Song, H., Kuykendall, T. & Yang, P. Platonic gold nanocrystals. *Angew. Chem., Int. Ed.* 43, 3673-3677 (2004).
23. Song, H., Kim, F., Connor, S., Somorjai, G. A. & Yang, P. Pt nanocrystals: Shape control and Langmuir-Blodgett monolayer formation. *J. Phys. Chem. B* 109, 188-193 (2005).
24. Tao, A., Sinsermsuksakul, P. & Yang, P. Polyhedral silver nanocrystals with distinct scattering signatures. *Angew. Chem., Int. Ed.* 45, 4597-4601 (2006).
25. Chen, J., Herricks, T. & Xia, Y. Polyol synthesis of platinum nanostructures: Control of morphology through the manipulation of reduction kinetics. *Angew. Chem., Int. Ed.* 44, 2589-2592 (2005).
26. Sau, T. K. & Murphy, C. J. Room temperature, high-yield synthesis of multiple shapes of gold nanoparticles in aqueous solution. *J. Am. Chem. Soc.* 126, 8648-8649 (2004).
27. Wiley, B., Sun, Y., Mayers, B. & Xia, Y. Shape-controlled synthesis of metal nanostructures: The case of silver. *Chem. Eur. J.* 11, 454-463 (2005).
28. Murphy, C. J. & Jana, N. R. Controlling the aspect ratio of inorganic nanorods and nanowires. *Adv. Mater.* 14, 80-82 (2002).
29. Gole, A. & Murphy, C. J. Seed-Mediated Synthesis of Gold Nanorods: Role of the Size and Nature of the Seed. *Chem. Mater.* 16, 3633-3640 (2004).
30. Yong, K.-T. et al. Shape Control of PbSe Nanocrystals Using Noble Metal Seed Particles. *Nano Lett.* 6, 709-714 (2006).
31. Sun, Y., Yin, Y., Mayers, B. T., Herricks, T. & Xia, Y. Uniform Silver Nanowires Synthesis by Reducing AgNO<sub>3</sub> with Ethylene Glycol in the Presence of Seeds and Poly(Vinyl Pyrrolidone). *Chem. Mater.* 14, 4736-4745 (2002).
32. Lee, H. et al. Morphological control of catalytically active platinum nanocrystals. *Angew. Chem., Int. Ed.* 45, 7824-7828 (2006).
33. Banse, B. A. & Koel, B. E. Interaction of oxygen with palladium(111): High effective oxygen pressure conditions by using nitrogen dioxide. *Surf. Sci.* 232, 275-85 (1990).
34. Somorjai, G. A. Introduction to surface chemistry and catalysis (John Wiley & Sons, Inc., New York, 1994).
35. Veisz, B. & Kiraly, Z. Size-Selective Synthesis of Cubooctahedral Palladium Particles Mediated by Metallomicelles. *Langmuir* 19, 4817-4824 (2003).
36. Pileni, M.-P. The role of soft colloidal templates in controlling the size and shape of inorganic nanocrystals. *Nat. Mater.* 2, 145-150 (2003).

37. Johnson, C. J., Dujardin, E., Davis, S. A., Murphy, C. J. & Mann, S. Growth and form of gold nanorods prepared by seed-mediated, surfactant-directed synthesis. *J. Mater. Chem.* 12, 1765-1770 (2002).
38. Lamy, C. & Leger, J. M. Electrocatalytic oxidation of small organic molecules at platinum single crystals. *J. Chim. Phys.* 88, 1649-71 (1991).
39. Markovic, N. M. & Ross, P. N. Surface science studies of model fuel cell electrocatalysts. *Surf. Sci. Rep.* 45, 117-229 (2002).
40. Baldauf, M. & Kolb, D. M. Formic Acid Oxidation on Ultrathin Pd Films on Au(*hkl*) and Pt(*hkl*) Electrodes. *J. Phys. Chem.* 100, 11375-11381 (1996).
41. Hoshi, N., Kida, K., Nakamura, M., Nakada, M. & Osada, K. Structural Effects of Electrochemical Oxidation of Formic Acid on Single Crystal Electrodes of Palladium. *J. Phys. Chem. B* 110, 12480-12484 (2006).
42. Niesz, K., Grass, M. & Somorjai, G. A. Precise Control of the Pt Nanoparticle Size by Seeded Growth Using EO<sub>13</sub>PO<sub>30</sub>EO<sub>13</sub> Triblock Copolymers as Protective Agents. *Nano Lett.* 5, 2238-2240 (2005).

**Acknowledgements**

This work was supported by the U.S. Department of Energy under Contract # DE-AC02-05CH11231. All TEM investigations, with the exception of those done on the Tecnai G<sup>2</sup> S-Twin, were performed at the National Center for Electron Microscopy, Lawrence Berkeley National Lab. We would also like to thank T. R. Kuykendall for the SEM work.

Correspondence and requests for materials should be addressed to P. Y. (p\_yang@berkeley.edu).

Supplementary Information accompanies this paper on [www.nature.com/naturematerials](http://www.nature.com/naturematerials).

**Competing financial interests**

The authors declare no competing financial interests.